

The structure of approximate two electron wavefunctions in intense laser driven ionization dynamics

Takeshi Sato* and Kenichi L. Ishikawa†

Photon Science Center, School of Engineering, The University of Tokyo,
7-3-1 Hongo, Bunkyo-ku, Tokyo 113-8656, Japan and

Department of Nuclear Engineering and Management, School of Engineering,
The University of Tokyo, 7-3-1 Hongo, Bunkyo-ku, Tokyo 113-8656, Japan

The structure of approximate two electron wavefunction is deeply investigated, both theoretically and numerically, in the strong-field driven ionization dynamics. Theoretical analyses clarify that for two electron singlet systems, the previously proposed time-dependent extended Hartree-Fock (TD-EHF) method [Phys. Rev. A **51**, 3999 (1995)] is equivalent to the multiconfiguration time-dependent Hartree-Fock method with two occupied orbitals. The latter wavefunction is further transformed into the natural expansion form, enabling the direct propagation of the natural orbitals (NOs). These methods, as well as the conventional time-dependent Hartree-Fock (TDHF) method, are numerically assessed for the description of ionization dynamics of one-dimensional helium atom model. This numerical analysis (i) explains the reason behind the well-known failure of TDHF method to describe tunneling ionization, (ii) demonstrates the interpretive power of the TD-EHF wavefunction both in the original nonorthogonal and the NO-based formulations, and (iii) highlights different manifestations of the electron correlation (effect beyond the single determinant description), in tunneling ionization, high harmonic generation, and nonsequential double ionization. Possible extensions of the NO basis approach to multielectron systems are briefly discussed.

I. INTRODUCTION

Tunneling ionization (TI) is one of the most important processes in the fields of high-field and ultrafast physics. It is a purely quantum mechanical effect, where electrons in an atom or molecule escape the binding potential with a finite probability by tunneling through the potential barrier distorted by an intense electromagnetic field. In case of an oscillating field, the ejected electron, feeling a reverse acceleration, may return to the core region, possibly undergoing recombination with the parent ion, or recollision with it to induce further excitation or ionization. These electron dynamics in the ultra-short, intense, and oscillating fields induce a variety of important nonlinear, nonperturbative phenomena, such as high harmonic generation (HHG) and nonsequential double ionization (NSDI).

Although the time-dependent Schrödinger equation (TDSE) provides the rigorous theoretical framework [within a single atom (molecule) response] for investigating such electron dynamics [1–16], direct applications of TDSE for systems with more than two electrons are extremely difficult. Therefore, the single-active electron (SAE) approximation has been widely used, in which only the outermost electron is explicitly treated, with the effect of all the other electrons embedded in a fixed model potential. This approximation, however, fails to account for multielectron effects in high-field phenomena. As a result, the correlated electron dynamics in, e.g., NSDI process is outside the scope of this approximation. Moreover, for the high-harmonic spectroscopy of multielectron dynamics in molecules [17–19], the effect of multichannel ionization has to be taken into account beyond the SAE picture.

A number of time-dependent wavefunction methods have been proposed to describe the multielectron dynamics in intense laser fields. The time-dependent Hartree-Fock (TDHF) method, which approximates the total wavefunction with a single determinant, was first applied to the ionization dynamics by Kulander [20]. Unfortunately as revealed by Pindzola *et al* [21], the TDHF method gives a qualitatively wrong description of the ionization process, despite the fact that the (time independent) HF method generally describes field-free ground-state of atoms and molecules quite well. A breakthrough was the introduction of the multiconfiguration time-dependent Hartree-Fock (MCTDHF) method [22, 23], which extends the wavefunction *ansatz* to the linear superposition of determinants with both expansion coefficients and constituent one electron wavefunctions (orbitals) treated as variational degrees of freedom. We recently proposed a more flexible time-dependent theory [24] based on the concept of complete-active-space self-consistent-field (CASSCF) originally developed in quantum chemistry [25], to extend the applicability of the MCTDHF method. See Ref. [24] for more comprehensive review of the proposed theoretical approaches including very recent developments.

With increase in expansion length, the MCTDHF method provides a powerful series of approximations from the single determinant TDHF to the exact TDSE limit. However, one should recognize that, apart from the severe exponential scaling of the computational cost against the system size, the interpretation of numerical results gets more and more difficult for simulations with higher accuracy, where the wavefunction is expanded with numerous determinants. It is, therefore, important to establish as simple an approximation as possible which captures essential features of electron dynamics while keeping the conceptual simplicity to allow for a clear interpretation of simulation results and deep insight into the physics involved.

In this work, we present theoretical and numerical in-

* Electronic mail: sato@atto.t.u-tokyo.ac.jp

† Electronic mail: ishiken@n.t.u-tokyo.ac.jp

vestigations on the structure of approximate two electron wavefunction—the simplest multielectron system—and their capability to describe intense laser driven ionization dynamics. We discuss the simplest form of the wavefunction required for a physically correct description of the TI process. Specifically, we focus on the time-dependent extended Hartree-Fock (TD-EHF) method [26–30], which approximates the total wavefunction by a symmetrized product of nonorthogonal orbitals [Eq. (6)]. We establish a transformation of the EHF wavefunction into a more convenient expression in terms of the orthonormal natural orbitals (NOs). This transformation enables the systematic improvement of approximations on top of the TD-EHF method, and also opens the possibility of its generalization to multielectron (beyond two electron) systems.

This paper is organized as follows. In Sec. II we theoretically investigate the TDHF and TD-EHF methods both in the original nonorthogonal as well as the NO-based formulations, and derive the equations of motion (EOMs) for the latter. Then in Sec. III, we apply various theoretical methods to the dynamics of one-dimensional helium model to investigate their performance in describing TI, HHG and NSDI processes. Finally, the summary of this work and some future prospects are given in Sec. IV. The Hartree atomic units are used throughout unless otherwise noted.

II. THEORETICAL ANALYSES OF THE TWO ELECTRON WAVEFUNCTION

A. RHF, UHF, and EHF wavefunctions

As mentioned in Sec. I, the TDHF method based on the the restricted HF (RHF) ansatz cannot describe the TI process correctly. For singlet two electron systems, the RHF wavefunction Ψ_{RHF} and the EOM for the orbital (TD-RHF) are given by,

$$\Psi_{\text{RHF}} = \|\psi_1(\mathbf{r}_1, t)\bar{\psi}_1(\mathbf{r}_2, t)\|, \quad (1)$$

$$i\dot{\psi}_1(\mathbf{r}, t) = [h(\mathbf{r}, t) + J[\psi_1](\mathbf{r})] \psi_1(\mathbf{r}, t), \quad (2)$$

respectively, where the symbol $\|\dots\|$ denotes a normalized Slater determinant, with ψ_1 ($\bar{\psi}_1$) being the direct product of a spatial orbital function $\psi(\mathbf{r})$ and an up (down) spin eigenfunction. The operator h is the one-electron part of the total Hamiltonian, and J is the Coulomb operator defined in Eq. (12). The TD-RHF method cannot describe the spatially different motions of the ionizing electron and that left in the ionic core, since it enforces the closed-shell structure.

One may consider that the single determinant unrestricted Hartree-Fock (UHF) wavefunction,

$$\Psi_{\text{UHF}} = \|\psi_1(\mathbf{r}_1, t)\bar{\psi}_2(\mathbf{r}_2, t)\|, \quad (3)$$

fits the purpose of describing the different motions of two electrons. However, if the initial two orbitals coincide, $\psi_1(\mathbf{r}, 0) = \psi_2(\mathbf{r}, 0)$, as is often the case for stable ground states with even number of electrons [31], these orbitals remain the same at any later time, $\psi_1(\mathbf{r}, t) = \psi_2(\mathbf{r}, t)$, unless

exposed to a spin-dependent perturbation. This is understood by seeing that the TD-UHF equations,

$$i\dot{\psi}_1(\mathbf{r}, t) = \{h(\mathbf{r}, t) + J[\psi_2]\} \psi_1(\mathbf{r}, t), \quad (4a)$$

$$i\dot{\psi}_2(\mathbf{r}, t) = \{h(\mathbf{r}, t) + J[\psi_1]\} \psi_2(\mathbf{r}, t), \quad (4b)$$

are symmetric for two spatial functions. Thus the TD-UHF approach cannot solve the problem of the TD-RHF method. More seriously, the UHF wavefunction is generally not the spin eigenfunction. The expectation value of the total spin operator is given by (assuming normalized orbitals)

$$\langle \Psi_{\text{UHF}} | S^2 | \Psi_{\text{UHF}} \rangle = 1 - |\langle \psi_1 | \psi_2 \rangle|^2. \quad (5)$$

If two orbitals are orthogonal, as expected, e.g., in the homogeneous dissociation of a hydrogen molecule or in the single ionization limit of helium, the UHF wavefunction corresponds to an equal weight mixture of singlet and triplet. The dynamics should be strongly altered by this spin contamination.

Clearly, the simplest allowed wavefunction capable of describing ionization processes consists of the symmetrized product of two different spatial orbitals,

$$\Psi_{\text{EHF}} = \frac{1}{\sqrt{2}} \{ \psi_1(\mathbf{r}_1, t)\psi_2(\mathbf{r}_2, t) + \psi_2(\mathbf{r}_1, t)\psi_1(\mathbf{r}_2, t) \}, \quad (6)$$

multiplied by a singlet spin function. Here ψ_1 and ψ_2 has to be nonorthogonal to seamlessly describe the closed-shell dominant ground state and open-shell dominant excited and continuum states. This form of wavefunction was used, in a phenomenological formulation, to explain the mechanism of NSDI [32]. In more rigorous variational treatments [26–30], this is often called the extended Hartree-Fock (EHF) wavefunction, and has been applied to electron dynamics of two electron systems. Although the same wavefunction has been sometimes called UHF wavefunction [26–28], we adopt the term EHF in this work to avoid confusion with the definition of the UHF in Eq. (3).

B. TD-EHF method

Following Tolley [28], but adopting concise notations of Nguyen and Bandrauk [30], the TD-EHF equation is written in the matrix form as follows;

$$i\dot{\mathbf{u}} = \{ (h - W)\mathbf{1} + \mathbf{S}^{-1}\mathbf{V} \} \mathbf{u}, \quad (7)$$

where \mathbf{u} is a column vector function with elements $\mathbf{u}(\mathbf{r}) = (\psi_2(\mathbf{r}), \psi_1(\mathbf{r}))^T$, $\mathbf{1}$ is a two by two unit matrix, and

$$\mathbf{S} = \begin{pmatrix} \langle \psi_1 | \psi_1 \rangle & \langle \psi_1 | \psi_2 \rangle \\ \langle \psi_2 | \psi_1 \rangle & \langle \psi_2 | \psi_2 \rangle \end{pmatrix} = \begin{pmatrix} 1 & \lambda \\ \lambda^* & 1 \end{pmatrix}, \quad (8)$$

$$\mathbf{V} = \begin{pmatrix} J[\psi_1] + K[\psi_1] & -\alpha_{12} \\ -\alpha_{21} & J[\psi_2] + K[\psi_2] \end{pmatrix}, \quad (9)$$

$$W = \frac{\langle \psi_1 \psi_2 | | \psi_1 \psi_2 \rangle - \lambda \langle \psi_2 \psi_2 | \psi_2 \psi_1 \rangle - \lambda^* \langle \psi_1 \psi_1 | \psi_1 \psi_2 \rangle}{\det(\mathbf{S})}, \quad (10)$$

where $\alpha_{12} = \langle \psi_1 \psi_1 | \psi_1 \psi_2 \rangle - W\lambda$, $\alpha_{21} = \langle \psi_2 \psi_2 | \psi_2 \psi_1 \rangle - W\lambda^*$, and $\langle \psi_1 \psi_2 | \psi_1 \psi_2 \rangle \equiv \langle \psi_1 \psi_2 | \psi_1 \psi_2 \rangle + \langle \psi_1 \psi_2 | \psi_2 \psi_1 \rangle$, with a shorthand notation for two electron repulsion integrals:

$$\langle \chi_1 \chi_2 | \chi_3 \chi_4 \rangle = \int d\mathbf{r}_1 d\mathbf{r}_2 \frac{\chi_1^*(\mathbf{r}_1) \chi_2^*(\mathbf{r}_2) \chi_3(\mathbf{r}_1) \chi_4(\mathbf{r}_2)}{|\mathbf{r}_1 - \mathbf{r}_2|}, \quad (11)$$

for a given orbital quartet $\chi_1, \chi_2, \chi_3, \chi_4$. The Coulomb J and exchange K operators appearing in Eq. (9) are defined by

$$J[\chi](\mathbf{r}) = \int d\bar{\mathbf{r}} \frac{\chi^*(\bar{\mathbf{r}}) \chi(\bar{\mathbf{r}})}{|\mathbf{r} - \bar{\mathbf{r}}|}, \quad (12)$$

$$(K[\chi]\psi)(\mathbf{r}) = \int d\bar{\mathbf{r}} \frac{\chi^*(\bar{\mathbf{r}}) \psi(\bar{\mathbf{r}})}{|\mathbf{r} - \bar{\mathbf{r}}|} \chi(\mathbf{r}), \quad (13)$$

for given orbitals χ and ψ . We have adopted the convention [26–28] that ψ_1 and ψ_2 are normalized, and nonorthogonal to each other with overlap $\langle \psi_1 | \psi_2 \rangle = \lambda$. Thus, the total wavefunction is not normalized but $\langle \Psi_{\text{EHF}} | \Psi_{\text{EHF}} \rangle = 1 + |\lambda|^2$. This is mathematically equivalent to an apparently different approach in Refs. [29, 30] where the orbitals are not normalized but the total wavefunction is normalized.

C. EHF wavefunction in terms of orthogonal orbitals

A problem of the TD-EHF method is the difficulty to improve the accuracy beyond a *single* antisymmetrized product in Eq. (6), due to the use of nonorthogonal orbitals. Thus it is desirable to formulate an equivalent theory in terms of orthogonal orbitals. To show that this is in fact possible, we apply the canonical orthogonalization to the nonorthogonal orbitals $\psi = (\psi_1, \psi_2)$ to obtain an orthonormal set $\phi = (\phi_1, \phi_2)$,

$$\phi(\mathbf{r}, t) = \psi(\mathbf{r}, t) \mathbf{X}(t), \quad \mathbf{X} = \mathbf{U} \mathbf{s}^{-1/2}, \quad (14)$$

where the unitary matrix \mathbf{U} diagonalizes the overlap matrix \mathbf{S} of Eq. (8) and \mathbf{s} is the diagonal matrix with elements being corresponding eigenvalues $s_{\pm} = 1 \pm |\lambda|$. Upon this transformation, the EHF wavefunction of Eq. (6) is expressed in terms of orthogonal orbitals $\{\phi_1, \phi_2\}$ as

$$\Psi_{\text{EHF}} = A_1(t) \|\phi_1(\mathbf{r}_1, t) \bar{\phi}_1(\mathbf{r}_2, t)\| - A_2(t) \|\phi_2(\mathbf{r}_1, t) \bar{\phi}_2(\mathbf{r}_2, t)\|, \quad (15)$$

where

$$A_1 = \frac{1 + |\lambda|}{\sqrt{2(1 + |\lambda|^2)}} \frac{\lambda^*}{|\lambda|}, \quad (16a)$$

$$A_2 = \frac{1 - |\lambda|}{\sqrt{2(1 + |\lambda|^2)}} \frac{\lambda}{|\lambda|}, \quad (16b)$$

$$\phi_1(\mathbf{r}) = \frac{1}{\sqrt{2(1 + |\lambda|)}} \left\{ \frac{\lambda}{|\lambda|} \psi_1(\mathbf{r}) + \psi_2(\mathbf{r}) \right\}, \quad (17a)$$

$$\phi_2(\mathbf{r}) = \frac{1}{\sqrt{2(1 - |\lambda|)}} \left\{ \psi_1(\mathbf{r}) - \frac{\lambda^*}{|\lambda|} \psi_2(\mathbf{r}) \right\}. \quad (17b)$$

Inversely, provided that the total wavefunction is given in the form of Eq. (15), it can be transformed back into Eq. (6) through $\psi(\mathbf{r}, t) = \phi(\mathbf{r}, t) \mathbf{X}^{-1}(t)$ as (assuming $|A_1| > |A_2|$)

$$\psi_1(\mathbf{r}) = \sqrt{\frac{1 + |\lambda|}{2}} \frac{\lambda^*}{|\lambda|} \phi_1(\mathbf{r}) + \sqrt{\frac{1 - |\lambda|}{2}} \phi_2(\mathbf{r}), \quad (18a)$$

$$\psi_2(\mathbf{r}) = \sqrt{\frac{1 + |\lambda|}{2}} \phi_1(\mathbf{r}) - \sqrt{\frac{1 - |\lambda|}{2}} \frac{\lambda}{|\lambda|} \phi_2(\mathbf{r}), \quad (18b)$$

$$\lambda = \frac{|A_1| - |A_2|}{|A_1| + |A_2|} \left(\frac{|A_2/A_1|}{|A_2/A_1|} \right)^{1/2}. \quad (18c)$$

The existence of the reversible map \mathbf{X} between the two expressions of the total wavefunctions, Eqs. (6) and (15), demonstrates that the electron dynamics can be equivalently represented with either expression. Thus instead of solving Eq. (7), we can formulate an equivalent theory by applying time-dependent variational method to Eq. (15) with both orbitals $\{\phi_1(t), \phi_2(t)\}$ and coefficients $\{A_1(t), A_2(t)\}$ treated as variational degrees of freedom. This will be done in Sec. II E after discussing the natural expansion of two electron wavefunctions.

D. Natural expansion of two electron wavefunction

The most general expansion of two electron wavefunction with given number, n , of orthonormal spatial orbitals is

$$\Psi_{\text{MC}} = \sum_{i=1}^n \sum_{j=1}^n C_{ij}(t) \|\phi'_i(\mathbf{r}_1, t) \bar{\phi}'_j(\mathbf{r}_2, t)\|. \quad (19)$$

This corresponds to the wavefunction used in the MCTDHF method. Now we show that this wavefunction can be reduced to the diagonal form:

$$\Psi_{\text{NO}} = \sum_{i=1}^n A_i(t) \|\phi_i(\mathbf{r}_1, t) \bar{\phi}_i(\mathbf{r}_2, t)\|, \quad (20)$$

in the case of singlet. The proof is made by noting that the matrix \mathbf{C} with elements C_{ij} in Eq. (19) is complex symmetric, thus can always be factorized to the diagonal form \mathbf{A} with diagonal elements A_i in Eq. (20), by Takagi's factorization [33, 34]:

$$\mathbf{C} = \mathbf{V} \mathbf{A} \mathbf{V}^T, \quad \mathbf{A} = \mathbf{V}^\dagger \mathbf{C} \mathbf{V}^*, \quad (21)$$

where upper scripts T, †, and * stand for transpose, Hermitian conjugate, and complex conjugate, respectively. Two sets of orthonormal orbitals in Eqs. (19) and (20) are connected by the unitary transformation \mathbf{V}

$$\phi_i(\mathbf{r}) = \sum_j \phi'_j(\mathbf{r}) V_{ji}. \quad (22)$$

The orbitals $\{\phi_i\}$ in Eq. (20) have a special significance of being the natural orbitals (NOs), i.e., diagonalize the first

order density matrix (1RDM):

$$\rho(\mathbf{r}_1, \mathbf{r}'_1) = 2 \int d\mathbf{r}_2 \Psi(\mathbf{r}_1, \mathbf{r}_2) \Psi^*(\mathbf{r}'_1, \mathbf{r}_2) \quad (23a)$$

$$= 2 \sum_{i=1}^n |A_i|^2 \phi_i(\mathbf{r}_1) \phi_i^*(\mathbf{r}'_1), \quad (23b)$$

and expansion coefficients are directly connected to the natural occupation numbers (eigenvalues of 1RDM),

$$\eta_i = 2|A_i|^2. \quad (24)$$

Hereafter we call $\{A_i\}$ the natural coefficients (NCs). The equivalence of Eqs. (6) and (15), as well as of Eqs. (19) and (20), are known in quantum chemistry [31, 35], for real stationary wavefunctions. Here we have explicitly shown that the same relations hold for arbitrary (both stationary and non-stationary) wavefunctions. In what follows, we will discuss the significance of these transformations in the time-dependent simulation and interpretation of two electron dynamics.

E. Direct propagation of natural orbitals

The natural expansion [Eq. (20)] is a special (NO) representation of the general MCTDHF wavefunction [Eq. (19)]. Therefore, the EOMs for the former wavefunction can be derived by using the invariance of the latter wavefunction with respect to the unitary transformation among the occupied orbitals. We first write down the MCTDHF equation [Eqs. (30) and (40) of Ref. [24], e.g.] for the two electron system;

$$i\dot{C}_{ij} = \sum_{kl} (h_{ik}\delta_{jl} + h_{jl}\delta_{ik} + \langle ij|kl \rangle) C_{kl}, \quad (25)$$

$$i\dot{\phi}_i = \hat{Q} \left(h\phi_i + \sum_j \Gamma_j \phi_j \rho_{ji}^{-1} \right) + \sum_{j \neq i} \phi_j R_{ji}, \quad (26)$$

where $h_{ij} = \langle \phi_i | h | \phi_j \rangle$, $\langle ij|kl \rangle = \langle \phi_i \phi_j | \phi_k \phi_l \rangle$, $\hat{Q} \equiv 1 - \sum_j |\phi_j\rangle\langle \phi_j|$, $\Gamma_i \phi_i = 2 \sum_{jkl} W_{jk} \phi_l C_{ij}^* C_{lk}$, and

$$W_{ij}(\mathbf{r}) = \int d\bar{\mathbf{r}} \frac{\phi_i^*(\bar{\mathbf{r}}) \phi_j(\bar{\mathbf{r}})}{|\mathbf{r} - \bar{\mathbf{r}}|}. \quad (27)$$

In Eq. (26) the matrix R with elements $R_{ij} \equiv i\langle \phi_i | \dot{\phi}_j \rangle$ can be an arbitrary Hermitian matrix in the general MCTDHF formulation [24]. Here this freedom is used to impose a condition that the 1RDM in the orbital basis ρ_{ij} is kept diagonal, $d\rho_{ij}/dt = 0$ ($i \neq j$). Following Refs. [36, 37] which discuss the natural expansion of bosonic wavefunction, we obtain the EOMs for NCs and NOs as follows;

$$i\dot{A}_i = \sum_{j=1}^n (2\delta_{ij} h_{ii} + \langle ii|jj \rangle) A_j, \quad (28a)$$

$$i\dot{\phi}_i = \hat{Q} F_i \phi_i \eta_i^{-1} + \sum_{j \neq i} \phi_j R_{ji}, \quad (28b)$$

where

$$F_i \phi_i = h\phi_i \eta_i + 2 \sum_j W_{ij} \phi_j A_i^* A_j, \quad (29)$$

and the orbital rotation matrix R is identified as

$$R_{ij} = \frac{F_{ij} - F_{ji}^*}{n_j - n_i}, \quad F_{ij} = \langle \phi_i | F_j \phi_j \rangle. \quad (30)$$

For notational brevity, we call this approach TD-NO n , with n denoting the number of NOs. The orthogonal reformulation of the EHF wavefunction, Eq. (15), is a special case with $n = 2$. An important advantage of the TD-NO n is its capability of improving the accuracy by increasing n . Moreover it allows the extension to multielectron systems as discussed below in Sec. IV. We emphasize that all the methods discussed in this section are not phenomenological but based on the physically solid variational principle.

III. NUMERICAL ASSESSMENTS

In this section, we numerically investigate the various ansatz of two electron wavefunctions discussed in Sec. II. For this purpose, we use the one-dimensional helium (1D-He) model. The electronic Hamiltonian is given by

$$H = \sum_{p=1}^2 \left[-\frac{\partial^2}{\partial z_p^2} - \frac{2}{\|z_p\|} - z_p E(t) \right] + \frac{1}{\|z_1 - z_2\|}, \quad (31)$$

for two electronic coordinates z_1 and z_2 , where the nuclear potential is centered at the origin, and soft Coulombic operator $1/\|x\| \equiv 1/\sqrt{x^2 + 1}$ is used both for nucleus-electron and electron-electron interactions. The electron-laser interaction is included within the dipole approximation and in the length gauge. Note that all the methods examined in this work are gauge-invariant as discussed, e.g., in Ref. [24]. In all simulations, spatial functions are discretized on equidistant grid points with spacing $\Delta z = 0.4$ within a simulation box $-1000 < z < 1000$. An absorbing boundary is implemented by a mask function of $\cos^{1/4}$ shape at 10% side edges of the box. Each EOM is solved by the fourth-order Runge-Kutta method with a fixed time step size (1/10000 of an optical cycle). The kinetic energy operator is evaluated by the eighth-order finite difference, and spatial integrations are performed by the trapezoidal rule. The initial (ground state) wavefunction is obtained by the imaginary time propagation of EOMs for each method.

A. Comparison of TD-RHF and TD-EHF methods

First we assess the performance of TD-RHF and TD-EHF methods by using numerically exact TDSE simulation as a reference. By doing so, we discuss the physical origin behind the well-known failure of the TD-RHF method in describing the TI. We used a six-cycle laser pulse of wavelength 780 nm and intensity 8×10^{14} W/cm² with a trapezoidal envelope (turning

on and off linearly within two cycles). This is the same laser profile as used in Ref. [29].

In Fig. 1 we show the evolution of the expectation values of the dipole moment (a), the velocity (b), and the acceleration (c) of electrons defined as follows:

$$\langle z \rangle = \langle \Psi | \sum_{i=1}^2 z_i | \Psi \rangle, \quad (32a)$$

$$\frac{d\langle z \rangle}{dt} = -i \langle \Psi | \sum_{i=1}^2 \frac{\partial}{\partial z_i} | \Psi \rangle, \quad (32b)$$

$$\frac{d^2\langle z \rangle}{dt^2} = \langle \Psi | \sum_{i=1}^2 \left[\frac{z_i}{\|z_i\|^2} + E(t) \right] | \Psi \rangle, \quad (32c)$$

where the Ehrenfest expressions are used for the velocity and the acceleration.

As seen in the figure, the TD-RHF method underestimates the oscillation amplitude of both dipole and dipole velocity compared to those of TDSE. For the dipole acceleration, the TD-RHF method underestimates the amplitude of the oscillation synchronized to the laser electric field, while exaggerates the higher order (higher frequency) response at the later stage of the pulse. In contrast, the TD-EHF results show reasonable agreement with TDSE ones for these quantities.

To clarify the qualitative difference of TD-RHF and TD-EHF results in Fig. 1, we perform the orbital decomposition analysis of the one electron probability density $\rho(z) \equiv 2 \int dz' |\Psi(z, z')|^2$ for the EHF wavefunction:

$$\rho(z) = \rho_1(z) + \rho_2(z) + \rho_{12}(z), \quad (33)$$

where $\rho_1 \equiv |\psi_1|^2/(1 + |\lambda|^2)$, $\rho_2 \equiv |\psi_2|^2/(1 + |\lambda|^2)$, and $\rho_{12} \equiv 2\text{Re}[\psi_1(z)\psi_2^*(z)\lambda]/(1 + |\lambda|^2)$. Accordingly, the expectation value of any local one-electron operator h is decomposed into contributions from each orbital $\langle h \rangle_1 = \text{tr}[h\rho_1]$, $\langle h \rangle_2 = \text{tr}[h\rho_2]$, and cross term $\langle h \rangle_{12} = \text{tr}[h\rho_{12}]$.

Figure 2 shows such a decomposition of the TD-EHF dipole moment, $\langle z \rangle = \langle z \rangle_1 + \langle z \rangle_2 + \langle z \rangle_{12}$. One immediately finds that the large amplitude motion at $t > 2.5T$ is dominated by the ψ_2 's contribution, while the orbital ψ_1 remains localized. Since two orbitals overlap only weakly in this time region, $\langle z \rangle_1$ and $\langle z \rangle_2$ can be interpreted as mean positions of an electron in ψ_1 and ψ_2 , respectively, i.e., the core electron and tunnel-ionizing electron. In this situation, where $\lambda \equiv \langle \psi_1 | \psi_2 \rangle \approx 0$, and the effect of exchange potential K is negligible in Eqs. (7)-(9), the ionizing electron in the outer orbital ψ_2 feels the nuclear potential screened by the core electron in the inner orbital ψ_1 ;

$$V_{\text{eff}}(z) = -\frac{2}{\|z\|} + J[\psi_1(t)](z), \quad (34)$$

which, due to the localization of the inner orbital (Fig. 2), asymptotically approaches to the cationic potential $V_{\text{eff}}(z) \rightarrow -1/|z|$ in the single ionization limit.

This is completely different from the TD-RHF picture, which forces two electrons to travel on the same orbital evolving in the field of nuclear potential screened only inefficiently

by the self Coulomb potential [Eq. (2)], thus fails to distinguish the core and ionizing electrons. Effectively this causes the decreased (increased) probability density $\rho(z)$ at large (small) $|z|$ regions compared to the exact density, leading the underestimation of the dipole and dipole velocity [Fig. 1 (a,b)]

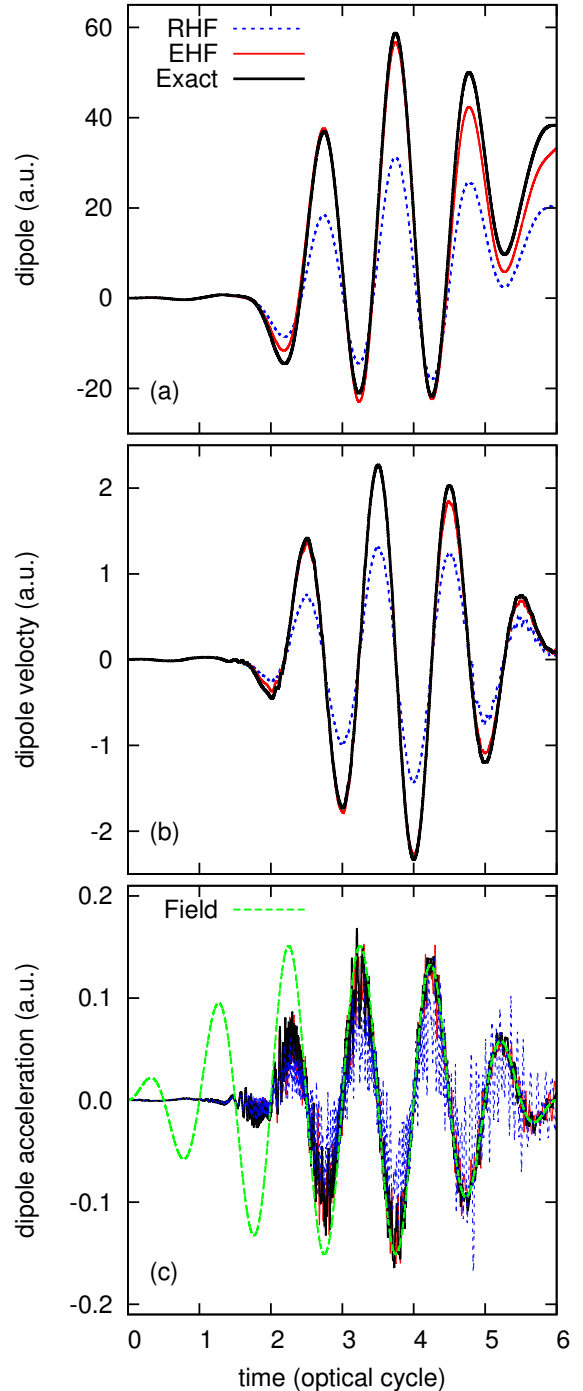


FIG. 1. Time evolution of the (a) dipole, (b) velocity, and (c) acceleration of electrons computed with TD-RHF, TD-EHF, and TDSE methods. The laser electric field $E(t)$ is also shown to be compared with the oscillation of acceleration.

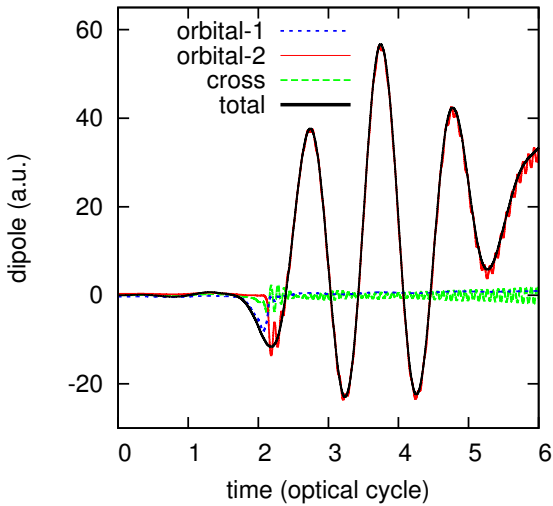


FIG. 2. Orbital decomposition of the dipole moment of TD-EHF method. Shown are the contributions from each orbital $\langle z \rangle_1$ and $\langle z \rangle_2$ (orbital-1 and orbital-2, respectively), the cross term $\langle z \rangle_{12}$ (cross) and the total sum, as a function of time. See text for more details.

which is dominated by the motion of the ionizing electron at large $|z|$, as well as the enhanced higher order response in the dipole acceleration [Fig. 1 (c)] to which the core electron at small $|z|$ contributes strongly.

B. Interpretation of EHF orbitals in tunneling ionization

Next in Fig. 3, we look into the time evolution of the non-orthogonal EHF orbitals. The initial orbitals [top panel of Fig. 3], start to oscillate following the laser field. Until around $t < 1.5T$, the oscillation is small in magnitude (relative to the scale of Fig. 3 at $t > 0$), and leads to only marginal ionization, keeping the relative “left” (orbital-1) and “right” (orbital-2) location of two orbitals. At $t = 1.75T$ when the laser force points to the negative direction of z -axis with $\sim 90\%$ of the maximum intensity, the “left” tail of the orbital-1 deforms appreciably, leading the first significant tunneling ionization at around $t = 2T$ when the laser force vanishes. Curiously at the first look, the outgoing part of orbital-1 (red) at $t = 2T$ looks replaced by the delocalized orbital-2 (black) at $t = 2.25T$. A closer inspection of the orbital evolution within this time region (Fig. 4) shows that there occurs a strong mixing and character change between two orbitals. This effect is also visible in the orbital components of the dipole in Fig. 2.

After the character mixing, the two orbitals get clearly characterized as “inner” (red) and “outer” (black) orbitals, the former being localized at origin, while the latter being delocalized. At $t = 2.25T$, the “right” tail of the outer orbital deforms toward positive direction, while the left-going part of the orbital loses stream feeling the reverse acceleration. At another 1/4 cycle later ($t = 2.5T$) when the laser force vanishes again, the whole wave packet drives with a positive velocity, undergoing both tunneling ionization towards “right” and recombination or recollision at the origin from the “left”.

At $t = 2.75T$, one sees a mirrored situation of that at half cycle before, namely, deformation of the “left” tail and nearly standing “right” wave packet. Then at $t = 3T$ the outer orbital represents both tunneling ionization towards “left” and recombination/recollision from the “right”. During the latter

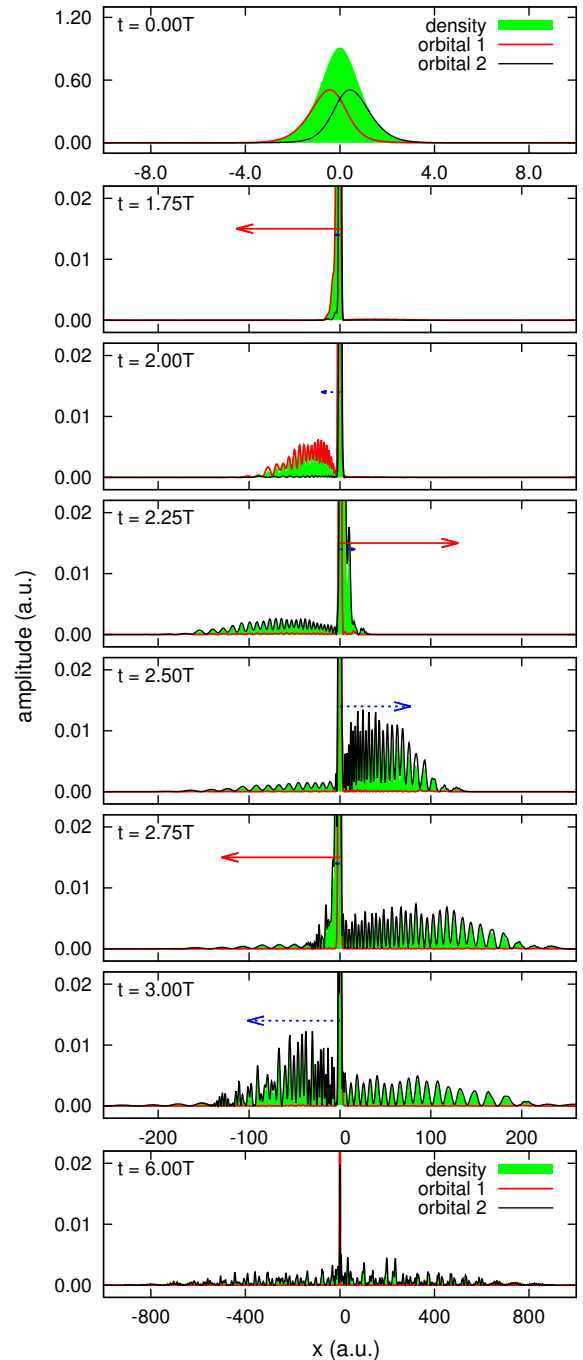


FIG. 3. Snapshots of evolving EHF orbitals at several instances of time. Note the different length scales for the initial (top), the final (bottom), and the intermediate (middles) times. The one electron probability density is also given by the filled region. The solid (red) and break (blue) arrows indicate the field force $-E(t)$ and the expectation value of the velocity $\langle \dot{z} \rangle$, respectively, in an arbitrary unit.

half of the pulse ($3T < t < 6T$), the ionizing electron in the outer orbital evolves like a single active electron feeling the screened nuclear potential V_{eff} of Eq. (34), resulting in the wide spread continuum state at the end of the pulse [bottom of Fig. (3)].

These analyses of EHF orbitals demonstrate the interpretive power of the TD-EHF method, which provides intuitive picture for the TI event and subsequent electron dynamics compatible to the semi-classical three step model [38]. Now we point out that the same picture can be drawn from computationally more convenient TD-NO2 method as shown in Fig. 4. Here we solve Eq. (28) for NCs $\{A_1, A_2\}$ and NOs $\{\phi_1, \phi_2\}$, from which the non-orthogonal orbitals $\{\psi_1, \psi_2\}$ are computed at each time step using Eq. (18). The obtained instantaneous non-orthogonal orbitals, plotted with dashed lines in Fig. 4, perfectly match the EHF orbitals. This numerically confirms the equivalence of the two sets of equations Eq. (7)

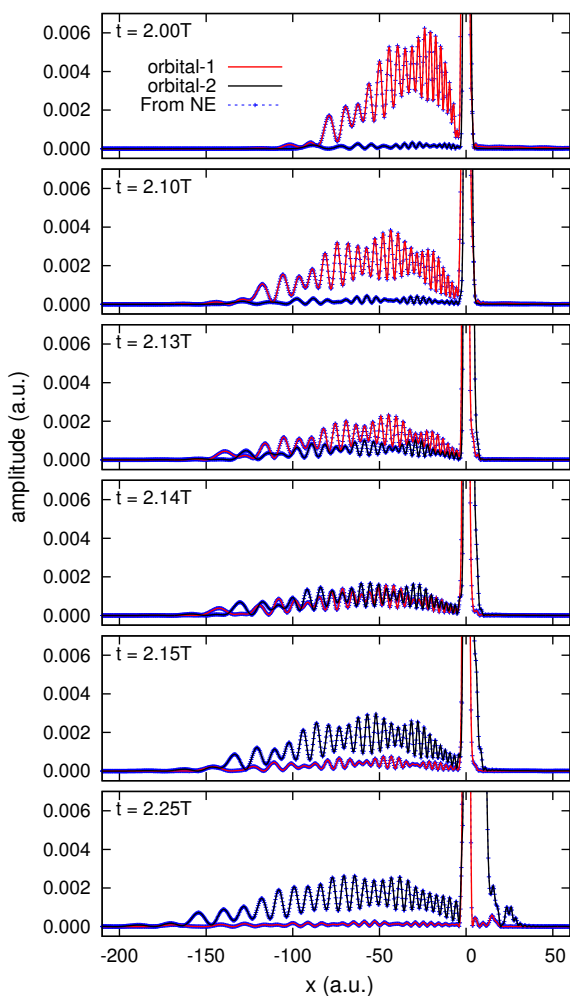


FIG. 4. Snapshots of evolving EHF orbitals at several moments of time within $2T \leq t \leq 2.25T$. The solid lines show two nonorthogonal orbitals directly propagated by the TD-EHF equation, Eq. (7). The dashed lines show nonorthogonal orbitals obtained by the transformation of Eq. (18), using NCs and NOs propagated by TD-NO2 equations, Eqs. (28a) and (28b).

and Eq. (28). The TD-NO2 method has some practical advantages over the TD-EHF method, e.g., allowing larger time steps and smaller simulation box sizes for the numerically convergent simulation. The direct propagation of nonorthogonal orbitals in the TD-EHF method, especially with unnormalized orbitals [29, 30], seems to occasionally cause numerical difficulties as shown in Appendix A.

C. High harmonic generation spectrum

Figure 5 compares the HHG spectra computed with TD-RHF, TD-NO2, TD-NO4, and TDSE methods. The spectrum is defined as the Fourier transform of the dipole acceleration in Eq. (32c) neglecting the bare field term. From a three-step model analysis [38] with Hartree-Fock-Koopmans ionization potential, the cutoff is predicted at about 103rd harmonic, in a good agreement with the TDSE spectrum.

As seen in the figure, the TD-RHF method overestimates the amplitude except for a first few harmonics. This reflects the enhanced high order responses in the dipole acceleration in Fig. 1 (c), caused by unphysical closed-shell description of two electrons. The panel (b) shows the perfect agreement between TD-EHF and TD-NO2 results, again confirming the equivalence of these theories. The TD-NO2 (TD-EHF) spec-

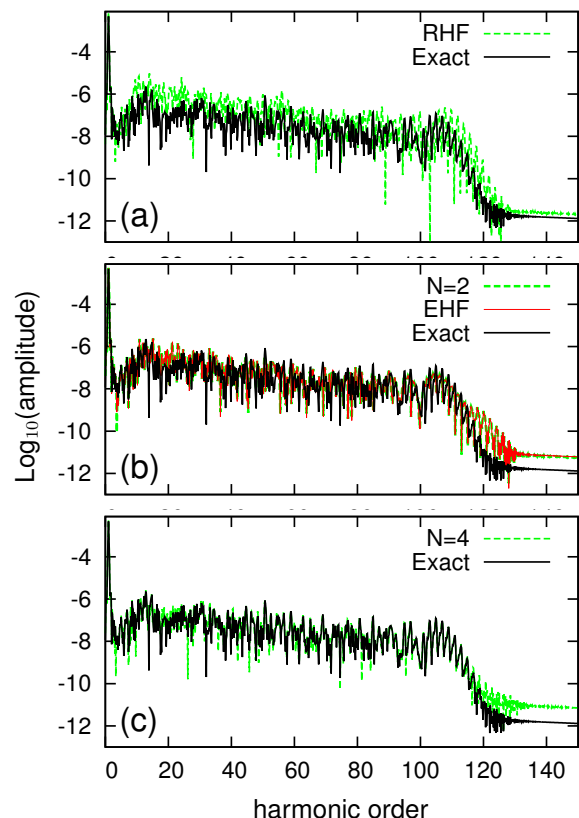


FIG. 5. HHG spectra obtained by TD-RHF (a), TD-EHF/TD-NO2 (b), and TD-NO4 (c) methods. The TDSE spectrum is shown in each panel for comparison.

trum shows a better agreement with the TDSE one, than the TD-RHF spectrum, both in the amplitude on the plateau and in the cutoff position. However, it fails to reproduce finer structures in the spectrum, especially at and beyond the cutoff frequency. It is always difficult to make a confident prediction of a given observable with a single approximate method. In this respect, the possibility of the systematic improvement in the TD-NO n series of approaches is highly appreciated, allowing a convergence study and self checking on the validity of the approximation. The TD-NO4 spectrum in Fig. 5 (c) shows a quite good agreement with the exact one.

D. Nonsequential double ionization

The HHG spectrum, and all the one particle properties investigated thus far, are not very sensitive to the individual motion of electrons since they depend only on the average motion of two electrons. To make a severer assessment on the quality of the two electron wavefunction, we investigate the NSDI process, which crucially depends on the motion of each electron. The TD-EHF method has been applied to the NSDI of 1D-He [29] and 1D-hydrogen molecule [30] models. Here we extend these previous works to take deeper account of roles of the electron correlation. We used a three cycle pulse with wavelength 750 nm, \sin^2 envelope, and intensities varied from 2×10^{14} to 3×10^{15} W/cm 2 . Following Refs. [29, 30], the ionization yields are estimated from the two electron probability $\rho(z_1, z_2) = \Psi(z_1, z_2)\Psi^*(z_1, z_2)$ as

$$P_0 = \int_{|z_1| < R} dz_1 \int_{|z_2| < R} dz_2 \rho(z_1, z_2), \quad (35a)$$

$$P_1 = 2 \int_{|z_1| > R} dz_1 \int_{|z_2| < R} dz_2 \rho(z_1, z_2), \quad (35b)$$

$$P_2 = \int_{|z_1| > R} dz_1 \int_{|z_2| > R} dz_2 \rho(z_1, z_2), \quad (35c)$$

where P_0 , P_1 , and P_2 are interpreted as zero (no ionization), single, and double ionization probabilities, respectively, with $R = 18$.

Figure 6 shows the intensity dependence of P_1 and P_2 at the end of the pulse. In accordance with previous 1D simulations with longer pulses [29, 30], the present simulation properly reproduces the experimental features; the exact (TDSE) result shows the “shoulder” like enhancement relative to the sequential result at the intensity region $0.8 \times 10^{14} \sim 1.5 \times 10^{15}$ W/cm 2 (shoulder region). The TD-RHF gives radically different results for both P_1 and P_2 compared to the TDSE results, with P_1 strongly underestimated while P_2 unphysically overestimated at and above the shoulder region. Both of these wrong behaviors originate from the closed-shell ansatz of Eq. (1), which in the first place cannot distinguish sequential and nonsequential processes. The TD-NO n series show a rapid convergence for P_1 as is the case for the one-particle observables in preceding sections. The TD-NO4 method already gives a nearly convergent curve of P_1 against the intensity, with relative deviations from the TDSE values less than 5.5%.

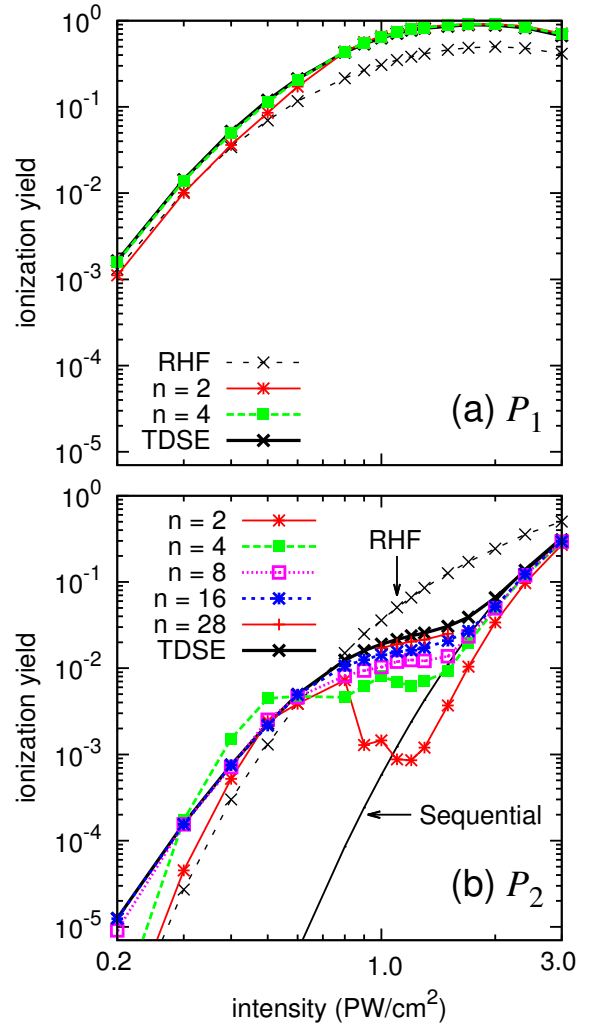


FIG. 6. Single and double ionizations of 1D-He obtained by various methods. Single (a) and (b) double ionization probabilities as a function of peak intensity. Also shown in (b) is the ionization probability of He $^+$, corresponding to the sequential model prediction of the double ionization probability.

In a striking contrast, Fig. 6 (b) reveals the extremely slow convergence of P_2 with respect to the number of NOs. Although the P_2 curve of the TD-NO2 method at least reproduces the shoulder feature, the P_2 values at around 10^{15} W/cm 2 are underestimated by an order of magnitude. A moderate overall accuracy is first achieved by TD-NO8, albeit with a sizable error at the shoulder region. The largest relative deviations of TD-NO n values of P_2 from the TDSE one within the shoulder region are 74%, 55%, 32%, and 18% with $n = 4, 8, 16,$ and 28 , respectively. Such slow convergence is a consequence of highly correlated electron dynamics involved in the NSDI; the recollision between the returning electron and parent ion requires precise account of instantaneous, short-range electron-electron correlation.

The recollision induced NSDI process can be separated into (i) the direct recollisional ionization, dominant at the shoulder region and (ii) recollision-excitation and subsequent tunneling

ionization, dominant at lower intensities. In the first mechanism, the high kinetic energy of the returning electron permits a closer approach [than in the mechanism (ii)] of electrons surpassing the electron-electron repulsive potential, and the direct energy transfer through the potential. This causes the especially slow convergence at the shoulder region. On the other hand, the lower energy inelastic collision in the second mechanism prevents two electrons from coming too close [in contrast to the mechanism (i)]. This is reflected by a faster convergence of P_2 values at lower intensities in Fig. 6 (b). The convergence becomes faster again at the highest intensities, where the electron-electron interaction is less important relative to the strong electron-laser interaction.

E. Roles of electron correlation in TI, HHG, and NSDI

Finally in this section, we summarize different roles of the electron correlation in TI, HHG, and NSDI processes. Figure 7 (a) shows the intensity dependence of the natural occupation numbers (ONs). The ONs $\{\eta_i\}$ are calculated at the end of the pulse of Sec. III D, by Eq. (24) for TD-NO n , or by diagonalizing the grid representation of the 1RDM [Eq. (23a)] for TDSE. As clearly seen in the figure except for TDHF, the first two ONs experience a drastic change, with decreasing (increasing) population for the initially strongly (weakly) populated first (second) natural orbital.

In TD-NO2, the weak ($\eta_1 \gg \eta_2$) and high ($\eta_1 \simeq \eta_2$) intensity limits of two ONs correspond, respectively, to the strongly overlapping ($|\langle\psi_1|\psi_2\rangle| \simeq 1$) and nearly orthogonal ($|\langle\psi_1|\psi_2\rangle| \simeq 0$) EHF orbitals as followed from Eq. (18). Physically, this represents the transition, during the course of increasing intensity, from the limit of no ionization to the other limit of completed single ionization. The same transition in the time domain is nothing but the TI process (in a sufficiently strong field), and the TDHF method cannot describe this transition. Thus, the electron correlation (effects beyond the single determinant description) is first manifested in the TI process itself; the breakdown of initial closed-shell symmetry.

Figure 7 (b) shows the final ONs for the field intensity 10^{15} W/cm 2 , plotted in logarithmic scale in the descending order. The ON spectrum obviously changes the slope in the vicinity of η_4 , suggesting that a first few and remaining NOs play different roles. To understand this behavior, we directly see errors of one- and two-electron probability densities (hereafter called 1-density and 2-density, respectively) of TD-NO n compared to exact TDSE densities;

$$\delta\rho_n(z) \equiv \rho_n(z) - \rho_\infty(z), \quad (36a)$$

$$\delta\rho_n(z_1, z_2) \equiv \rho_n(z_1, z_2) - \rho_\infty(z_1, z_2), \quad (36b)$$

where ρ_n (ρ_∞) is the density from TD-NO n (TDSE) wavefunction. The first and second entries of table I show the absolute error $|\delta\rho_n(z)|$ of 1-density integrated and normalized

over the inner ($|z| < R$) and outer ($|z| > R$) spatial regions;

$$\Delta_{<}^{(1)} = \frac{1}{N_{<}} \int_{|z|<R} dz |\delta\rho_n(z)|, \quad (37a)$$

$$\Delta_{>}^{(1)} = \frac{1}{N_{>}} \int_{|z|>R} dz |\delta\rho_n(z)|, \quad (37b)$$

where $N_{<}$ and $N_{>}$ are the norms of the exact 1-density $\rho_\infty(z)$ within inner and outer regions, respectively. Table I shows a rapid convergence of the 1-density, especially for the inner region. Therefore, we conclude that the first several NOs in Fig. 7 (b), before the slope change, are responsible for quantitative improvement of single electron dynamics (governed by 1-density) on top of the basic two orbital description of

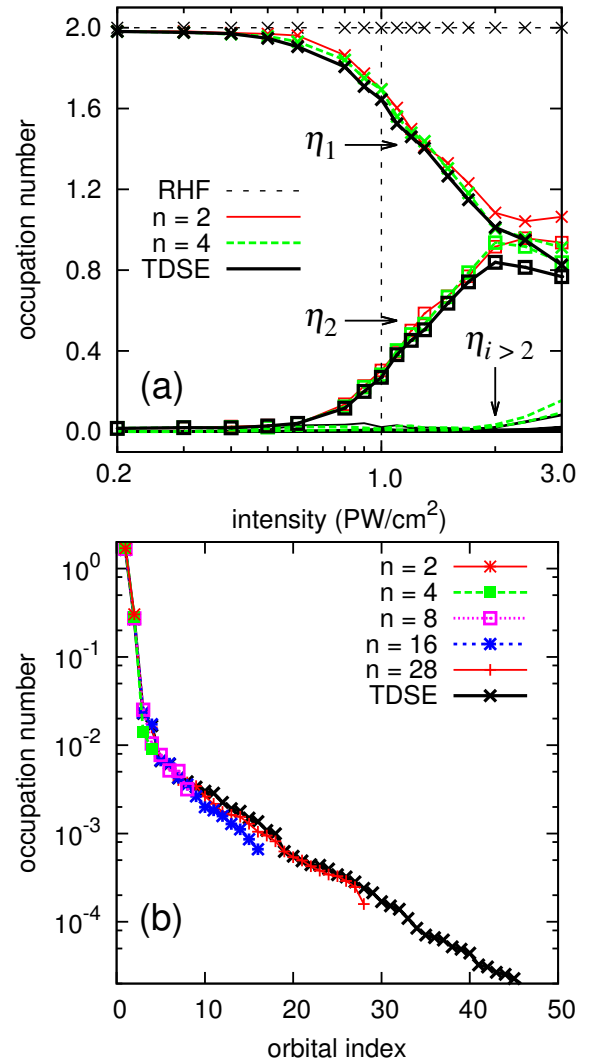


FIG. 7. (a) Natural occupation numbers (ONs) at the end of the pulse as a function of peak intensity. Shown are the available number of ONs; one for TD-RHF which is just a constant 2.0, n for TD-NO n , and 5000 (number of grid points) for TDSE methods. The first and second ONs are labeled with cross (\times) and square (\square) markers, respectively. (b) ONs plotted in the descending order for TD-NO n and TDSE methods at the end of the pulse of intensity 1 PW/cm^2 [indicated with the vertical line in (a)].

TABLE I. The domain divided relative errors (%) of 1-density ($\Delta^{(1)}$) and 2-density ($\Delta^{(2)}$) relative to the TDSE densities, at the end of the pulse with intensity 10^{15} W/cm². See text and Eqs. (37) and (38) for definition of $\Delta^{(1)}$ and $\Delta^{(2)}$. The inner ($N_{<}$) and outer ($N_{>}$) norms of the 1-density, and no (P_0), single (P_1), and double (P_2) ionization parts of 2-density are also shown for TDSE.

n	$\Delta_{<}^{(1)}$	$\Delta_{>}^{(1)}$	$\Delta_{<<}^{(2)}$	$\Delta_{><}^{(2)}$	$\Delta_{>>}^{(2)}$
RHF: 1	25.6	88.9	102.0	91.1	264.2
EHF: 2	11.6	23.9	35.3	28.5	96.8
4	5.4	10.8	16.0	17.7	94.8
8	1.9	4.1	6.7	9.2	81.6
12	1.2	3.0	4.5	6.3	73.9
16	0.9	2.4	3.6	5.0	62.9
20	0.7	1.9	2.1	4.3	55.2
28	0.3	1.1	1.6	2.6	36.9
	$N_{<}$	$N_{>}$	P_0	P_1	P_2
TDSE	1.332	0.668	0.351	0.630	0.019

TD-NO2 (or equivalently TD-EHF). As a consequence, one electron properties, including HHG spectrum, are described well by relatively small number of NOs.

Table I also lists domain divided relative errors of 2-density;

$$\Delta_{<<}^{(2)} = \frac{1}{P_0} \int_{|z_1| < R} dz_1 \int_{|z_2| < R} dz_2 |\delta\rho(z_1, z_2)|, \quad (38a)$$

$$\Delta_{><}^{(2)} = \frac{2}{P_1} \int_{|z_1| > R} dz_1 \int_{|z_2| < R} dz_2 |\delta\rho(z_1, z_2)|, \quad (38b)$$

$$\Delta_{>>}^{(2)} = \frac{1}{P_2} \int_{|z_1| > R} dz_1 \int_{|z_2| > R} dz_2 |\delta\rho(z_1, z_2)|, \quad (38c)$$

where P_i ($i = 0, 1, 2$) are the exact (TDSE) probabilities from Eq. (35). The quantities $\Delta_{<<}^{(2)}$, $\Delta_{><}^{(2)}$, and $\Delta_{>>}^{(2)}$ measure the accuracy of 2-density for electron pairs undergoing no, single, and double ionization. Table I clearly demonstrates slower convergence of 2-density than 1-density, especially for the doubly ionized pair of electrons. This reflects the strong short-range correlation in NSDI process as discussed in Sec. III D. Therefore, the totality of weakly populated NOs in Fig. 7 (b), after the slope change, contributes to the improvement in the description of the explicitly correlated relative motion of two electrons governed by 2-density.

IV. SUMMARY

This work addresses the structure of approximate two electron wavefunction required for properly describing intense laser driven ionization dynamics. We theoretically establish the equivalence of TD-EHF method and MCTDHF method with two occupied orbitals. The latter method is formulated in the form of natural expansion, allowing the direct propagation of NOs. The time-dependent NOs can be transformed back into the nonorthogonal EHF orbitals, thus combines the computational advantages of orthogonal orbitals and interpretive power of nonorthogonal orbitals.

Numerical application of TD-NO n approaches to 1D-He model highlights different manifestations of electron correlation. (i) The breaking closed-shell symmetry during the TI process, of which inclusion is essential (by TD-EHF or TD-NO2 as the simplest approximation) for a physically meaningful description. (ii) The correlation correction to the one electron density, (included by a few more orbitals) which quantitatively refines the description of single electron processes (in the presence of other electrons), thus important for accurate computations of one electron properties such as HHG. (iii) The instantaneous, short-range electron-electron correlation (requiring much more orbitals) involved in the recollision-induced NSDI process. The NO-based reformulation of the TD-EHF method enables such systematic evaluations of roles of electron correlation in TI, HHG, and NSDI processes, in a unified variational ansatz of Eq. (20).

There exists a promising extension of the NO-based approach to multielectron systems in the following form;

$$\Psi(\mathbf{x}_1, \mathbf{x}_2, \dots, \mathbf{x}_N) = \hat{A} \prod_{P=1}^{N/2} \psi_P(\mathbf{x}_{2P-1}, \mathbf{x}_{2P}), \quad (39)$$

where the N -electron wavefunction (assuming even N for simplicity) is given in terms of antisymmetrized product of *geminals* (two electron wavefunction), instead of orbitals as in TDHF method. Each geminal ψ_P can take the form of the natural expansion in Eq. (20). The geminal product wavefunction of Eq. (39) has a long history in the stationary quantum chemistry, particularly with the so called strong orthogonality condition [39, 40], known under the name of antisymmetrized products of strongly orthogonal geminals [40], or generalized valence-bond in the perfect-pairing approximation [41]. These methods are computationally far less demanding than configuration-based approaches like MCTDHF method, and at the same time, keep the conceptual simplicity of EHF wavefunction for two electron systems. A time-dependent theory based on Eq. (39) is now under development.

ACKNOWLEDGMENTS

This research is supported in part by Grant-in-Aid for Scientific Research (No. 23750007, No. 23656043, No. 23104708, No. 25286064, No. 26390076, and No. 26600111) from the Ministry of Education, Culture, Sports, Science and Technology (MEXT) of Japan, and also by Advanced Photon Science Alliance (APSA) project commissioned by MEXT. This research is also partially supported by the Center of Innovation Program from Japan Science and Technology Agency, JST.

Appendix A: Numerical stability of TD-EHF and TD-NO2 methods

As discussed in Secs. II B and II C, the TD-EHF method either with normalized orbitals [26–28] adopted in this work or with unnormalized orbitals [29, 30], and the TD-NO2 method

are mathematically equivalent. We found, however, that the propagation of TD-EHF equation, especially with unnormalized orbitals, requires severer simulation condition (larger simulation box and/or finer temporal step size). Figure 8 shows the dipole acceleration as a function of time with the same simulation condition as in Sec. III A except for the increased peak intensity of 3×10^{15} W/cm² and smaller simulation box, $|z| < 600$. The TD-EHF simulation with unnormalized orbitals uses EOMs given in Ref. [30]. It is confirmed that this box size is sufficient for obtaining the convergent acceleration value with TD-NO2. As seen in the figure the TD-EHF result with unnormalized orbitals begins to deviate from the other results after two optical cycles, and gets unstable after three cycles. This behavior originates from the presence of orbital overlap integrals in the TD-EHF equation [Eq. (7)]. It requires a precise conservation of orbital norms and mutual overlap *within* the simulation box (therefore necessitates a large box to support the outgoing electrons); otherwise the inaccurate \mathcal{S} matrix of Eq. (8) alters the dynamics even at the core region (responsible for the dipole acceleration). The normalized orbital approach of TD-EHF largely alleviates this problem since it only involves overlap $\lambda \equiv \langle \psi_1 | \psi_2 \rangle$ in Eq. (8) with each orbital *assumed* normalized.

In the TD-NO2 formulation, the orbital propagation is more stable since it utilizes the *assumed* orbital orthonormality, not involving box normalization in its EOM [Eq. (28b)]. Instead, the normalization of the total wavefunction is governed by the EOM for the NCs [Eq. (28a)], which is unitary irrespective of

a box truncation. As a result, the TD-NO approach allows a relatively small simulation box (with a good absorbing boundary) for the dynamics at the core region. It is also compatible to the advanced treatment of outgoing flux as developed in Ref. [42].

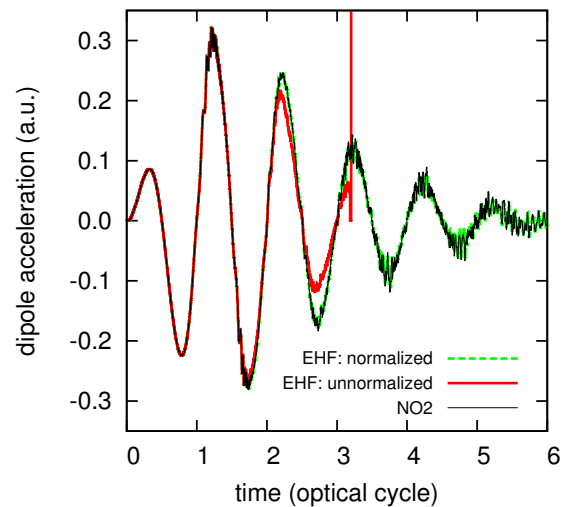


FIG. 8. Time evolution of the dipole acceleration in case of an increased peak intensity, 3×10^{15} W/cm² and a reduced box size. Results of TD-EHF with normalized and unnormalized orbitals, and TD-NO2.

-
- [1] M. S. Pindzola and F. Robicheaux, Phys. Rev. A **57**, 318 (1998).
 [2] M. S. Pindzola and F. Robicheaux, J. Phys. B **31**, L823 (1998).
 [3] J. Colgan, M. S. Pindzola, and F. Robicheaux, J. Phys. B **34**, L457 (2001).
 [4] J. S. Parker, L. R. Moore, K. J. Meharg, D. Dundas, and K. T. Taylor, J. Phys. B **34**, L69 (2001).
 [5] S. Laulan and H. Bachau, Phys. Rev. A **68**, 013409 (2003).
 [6] B. Piraux, J. Bauer, S. Laulan, and H. Bachau, Eur. Phys. J. D **26**, 7 (2003).
 [7] S. Laulan and H. Bachau, Phys. Rev. A **69**, 033408 (2004).
 [8] K. L. Ishikawa and K. Midorikawa, Phys. Rev. A **72**, 013407 (2005).
 [9] J. Feist, S. Nagele, R. Pazourek, E. Persson, B. I. Schneider, L. A. Collins, and J. Burgdörfer, Phys. Rev. Lett. **103**, 063002 (2009).
 [10] R. Pazourek, J. Feist, S. Nagele, E. Persson, B. I. Schneider, L. A. Collins, and J. Burgdörfer, Phys. Rev. A **83**, 053418 (2011).
 [11] K. L. Ishikawa and K. Ueda, Phys. Rev. Lett. **108**, 033003 (2012).
 [12] S. Sukiasyan, K. L. Ishikawa, and M. Ivanov, Phys. Rev. A **86**, 033423 (2012).
 [13] K. L. Ishikawa and K. Ueda, Appl. Sci. **3**, 189 (2013).
 [14] W. Vanroose, D. A. Horner, F. Martín, T. N. Rescigno, and C. W. McCurdy, Phys. Rev. A **74**, 052702 (2006).
 [15] D. A. Horner, S. Miyabe, T. N. Rescigno, C. W. McCurdy, F. Morales, and F. Martín, Phys. Rev. Lett. **101**, 183002 (2008).
 [16] T.-G. Lee, M. S. Pindzola, and F. Robicheaux, J. Phys. B **43**, 165601 (2010).
 [17] O. Smirnova, Y. Mairesse, S. Patchkovskii, N. Dudovich, D. Villeneuve, P. Corkum, and M. Y. Ivanov, Nature **460**, 7258 (2009).
 [18] O. Smirnova, S. Patchkovskii, Y. Mairesse, N. Dudovich, and M. Y. Ivanov, Proc. Natl. Acad. Sci. **106**, 16556 (2009).
 [19] Y. Mairesse, J. Higuier, N. Dudovich, D. Shafir, B. Fabre, E. Mevéll, and E. Constant, Phys. Rev. Lett. **104**, 21 (2010).
 [20] K. C. Kulander, Phys. Rev. A **36**, 2726 (1987).
 [21] M. S. Pindzola, D. C. Griffin, and C. Bottcher, Phys. Rev. Lett. **66**, 2305 (1991).
 [22] J. Caillat, J. Zanghellini, M. Kitzler, O. Koch, W. Kreuzer, and A. Scrinzi, Phys. Rev. A **71**, 012712 (2005).
 [23] T. Kato and H. Kono, Chem. Phys. Lett. **392**, 533 (2004).
 [24] T. Sato and K. L. Ishikawa, Phys. Rev. A **88**, 023402 (2013).
 [25] B. O. Roos, Adv. Chem. Phys. **69**, 399 (1987).
 [26] M. S. Pindzola, P. Gavras, and T. W. Gorczyca, Phys. Rev. A **51**, 3999 (1995).
 [27] M. S. Pindzola, F. Robicheaux, and P. Gavras, Phys. Rev. A **55**, 1307 (1997).
 [28] A. J. Tolley, J. Phys. B **32**, 3449 (1999).
 [29] N. E. Dahlen and R. van Leeuwen, Phys. Rev. A **64**, 023405 (2001).
 [30] N. A. Nguyen and A. D. Bandrauk, Phys. Rev. A **73**, 032708 (2006).
 [31] A. Szabo and N. S. Ostlund, *Modern Quantum Chemistry* (Dover, Mineola, 1996).
 [32] J. B. Watson, A. Sanpera, D. G. Lappas, P. L. Knight, and

- K. Burnett, Phys. Rev. Lett. **78**, 1884 (1997).
- [33] T. Takagi, Japanese J. Math **1**, 83 (1927).
- [34] A. Bunse-Gerstner and W. B. Gragg, J. Comput. Appl. Math **21**, 41 (1988).
- [35] W. Kutzelnigg, Theoret. Chim. Acta. **1**, 327 (1963).
- [36] A. P. J. Jansen, J. Chem. Phys. **99**, 4055 (1993).
- [37] U. Manthe, J. Chem. Phys. **101**, 2652 (1994).
- [38] P. B. Corkum, Phys. Rev. Lett. **71**, 1994 (1993).
- [39] T. Arai, J. Chem. Phys. **33**, 95 (1960).
- [40] W. Kutzelnigg, J. Chem. Phys. **40**, 3640 (1964).
- [41] W. J. Hunt, P. J. Hay, and W. A. Goddard, J. Chem. Phys. **57**, 738 (1972).
- [42] A. Scrinzi, New J. Phys. **14**, 085008 (2012).